where the symbol Σ'_n implies that the summation does not include $n=m$. On replacing the coefficients $C_{mn}(z')$ by the first three terms of its Taylor series expansion, a recurrence formula that expresses $f_m(z-\Delta z)$ in terms of $f_m(z)$ is obtained upon integration. Thus the solution of (A1) for the region $z_T > z > z_B$ is

$$f_m(p+1) = P_m^-(p+1/2)\left[f_m(p)P_m^+(p+1/2) + \sum_n{}' D_{mn}(p+1/2) f_n(p) P_n^+(p+1/2)\right] \quad \text{(A2)}$$

where

$$z_T = L - p\Delta z,$$
$$z_B = L - (p+1)\Delta z,$$
$$z_c = L - (p+1/2)\Delta z \quad \text{(A3)}$$

$$P_m^{\pm} = \exp\left[-\frac{\Delta z}{2}\left\{ C_{mn} \pm \frac{\Delta z}{4} C'_{mn} + \frac{(\Delta z)^2}{24} C''_{mm} \right\}\right] \quad \text{(A4)}$$

$$D_{mn} = -\Delta z \operatorname{sinc} \theta_{mn}\left[C_{mn} + \frac{i\Delta z}{2} C'_{mn} \frac{1-\theta_{mn}\cot\theta_{mn}}{\theta_{mn}} + \frac{(\Delta z)^2}{8} C''_{mn}\left\{ 1 - \frac{2(1-\theta_{mn}\cot\theta_{mn})}{\theta_{mn}^2}\right\}\right] \quad \text{(A5)}$$

and

$$\theta_{mn} = \frac{i\Delta z}{2}\left[C_{mm} - C_{nn}\right]. \quad \text{(A6)}$$

Acknowledgment

The authors wish to thank Mrs. E. Everett for typing the manuscript.

References

[1] M. Abramowitz and I. A. Stegun, *Handbook of Mathematical Functions with Formulas, Graphs and Mathematical Tables* (Applied Mathematics Series 55). Washington, DC: National Bureau of Standards, U.S. Government Printing Office, 1964.

[2] E. Bahar, "Generalized characteristic functions for simultaneous linear differential equations with variable coefficients applied to propagation in inhomogeneous anisotropic media," *Can. J. Phys.*, vol. 54, no. 3, pp. 301–316, 1976.

[3] E. Bahar and B. S. Agrawal, "A generalized WKB approach to propagation in inhomogeneous dielectric waveguides," *Radio Sci.*, vol. 12, no. 4, pp. 611–618, 1977.

[4] M. Hashimoto, "A perturbational method for the analysis of wave propagation in inhomogeneous dielectric waveguides with perturbed media," *IEEE Trans. Microwave Theory Tech.*, vol. MTT-24, pp. 559–566, 1976.

[5] ——, "Propagation of cladded inhomogeneous dielectric waveguides," *IEEE Trans. Microwave Theory Tech.*, vol. MTT-24, pp. 404–409, 1976.

[6] E. T. Kornhauser and A. D. Yaghjian, "Modal solution of a point source in a strongly focusing medium," *Radio Sci.*, vol. 2, no. 3, pp. 299–310, 1967.

Modal Analysis of Homogeneous Optical Fibers with Deformed Boundaries

EIKICHI YAMASHITA, MEMBER, IEEE, KAZUHIKO ATSUKI, OSAMU HASHIMOTO, AND KOUJI KAMIJO

***Abstract*—The modal characteristics of homogeneous optical fibers with several types of deformed boundaries are analyzed by a numerical method based on the point-matching principle. The propagation constants of various modes are given. The separation of degeneracy in the dominant mode is discussed. The results of microwave-model experiments show good agreement with those of calculation.**

Manuscript received March 16, 1978; revised August 22, 1978.

E. Yamashita and K. Atsuki are with the University of Electro-Communications, Tokyo, Japan.

O. Hashimoto is with Tokyo Shibaura Electric Company, Ltd., Tokyo, Japan.

K. Kamijo is with the Japan Broadcasting Corporation.

I. Introduction

With the recent development of communication techniques using low-loss optical fibers, it became important to investigate detailed electromagnetic fields and propagation characteristics of various optical fibers. We pay attention to modal characteristics of a class of optical fibers with deformed boundaries which would be caused in the process of fabrication. Many approximate methods have been recently applied to analyze graded index optical fibers. Yet, only a few papers have discussed the problem of deformed boundaries.

0018-9480/79/0400-0352$00.75

Yeh [1] has analyzed elliptical dielectric waveguides by deriving infinite determinants on hybrid modes. Schlosser [2] investigated a slightly elliptical dielectric wire by using the solution of the wave equation in the circular cylindrical coordinates. He also calculated the delay distortion of signals in glass fiber due to small elliptical deformations of boundaries [3]. Since wave equations are not separable except in eleven coordinate systems, numerical methods are required.

Goell [4] described a computer analysis of the propagating modes in rectangular dielectric waveguides. He expanded electromagnetic fields in terms of circular harmonics and employed the point-matching method to satisfy boundary conditions approximately. This approach is considered to be applicable to dielectric waveguides of other cross sections. James and Gallett [5] also pointed out the usefulness of this approach. Bird [6] has discussed guiding structures of polygonal boundaries based on the hybrid finite element method.

This paper describes the results of computer analyses on the propagation modes and electromagnetic fields of optical fibers with deformed boundaries by extending Goell's approach to more general cases. Microwave-model experiments that confirm our theoretical results are also described.

II. Method of Analysis

A circular dielectric waveguide has been rigorously analyzed by the method of separation of variables. As a result, the electromagnetic fields in the waveguide are expressed in terms of Bessel's functions, and those outside the waveguide are expressed in terms of modified Bessel's functions. The treatment of hybrid modes is necessary to satisfy the boundary conditions on the waveguide surface. The dominant mode of this waveguide is known as the HE_{11} mode and has no cutoff frequencies.

Numerical methods are required to analyze general boundaries. It is natural to use a linear combination of Bessel's functions in expressing electromagnetic fields of dielectric waveguides with boundaries close to circular. Therefore, the longitudinal components of the electric and magnetic fields can be written [5]

$$E_{z1} = \sum_{n=0}^{\infty} \left[a_n^s \sin(n\theta) + a_n^c \cos(n\theta) \right] J_n(hr) e^{j(\omega t - \beta z)} \quad (1)$$

$$H_{z1} = \sum_{n=0}^{\infty} \left[b_n^s \sin(n\theta) + b_n^c \cos(n\theta) \right] J_n(hr) e^{j(\omega t - \beta z)} \quad (2)$$

in the waveguide and

$$E_{z2} = \sum_{n=0}^{\infty} \left[c_n^s \sin(n\theta) + c_n^c \cos(n\theta) \right] K_n(pr) e^{j(\omega t - \beta z)} \quad (3)$$

$$H_{z2} = \sum_{n=0}^{\infty} \left[d_n^s \sin(n\theta) + d_n^c \cos(n\theta) \right] K_n(pr) e^{j(\omega t - \beta z)} \quad (4)$$

outside the waveguide where

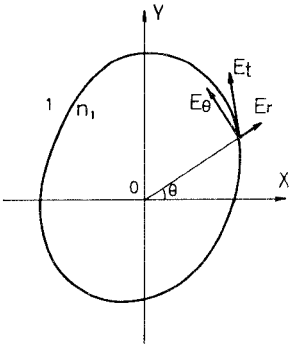

Fig. 1. Illustration of a tangential component of an electric field vector E_t, composed of the r-component E_r, and the θ-component E_θ: $\epsilon_1 = n_1^2 \epsilon_0$.

$$h^2 = k_1^2 - \beta^2 \quad (5)$$

$$p^2 = \beta^2 - k_0^2 \quad (6)$$

$$k_1^2 = \omega^2 \epsilon_1 \mu_0 \quad (7)$$

$$k_0^2 = \omega^2 \epsilon_0 \mu_0 \quad (8)$$

and $J_n(hr)$ and $K_n(pr)$ are Bessel's function and modified Bessel's function of the nth order, respectively.

The other field components are derived using Maxwell's equations

$$E_r = \frac{-j\beta}{k^2 - \beta^2} \left[\frac{\partial E_z}{\partial r} + \left(\frac{\omega \mu_0}{\beta r} \right) \frac{\partial H_z}{\partial \theta} \right] \quad (9)$$

$$E_\theta = \frac{-j\beta}{k^2 - \beta^2} \left[\frac{1}{r} \frac{\partial E_z}{\partial \theta} - \left(\frac{\omega \mu_0}{\beta} \right) \frac{\partial H_z}{\partial r} \right] \quad (10)$$

$$H_r = \frac{-j\beta}{k^2 - \beta^2} \left[-\left(\frac{k^2}{\omega \mu_0 \beta r} \right) \frac{\partial E_z}{\partial \theta} + \frac{\partial H_z}{\partial r} \right] \quad (11)$$

$$H_\theta = \frac{-j\beta}{k^2 - \beta^2} \left[\left(\frac{k^2}{\omega \mu_0 \beta} \right) \frac{\partial E_z}{\partial r} + \frac{1}{r} \frac{\partial H_z}{\partial \theta} \right] \quad (12)$$

where $k = k_1$ in the waveguide and $k = k_0$ outside the waveguide. The boundary conditions imposed on fields are the continuation of tangential components. The tangential components of fields at any boundary point can be expressed by combining the r- and θ-components of the field. This is illustrated in Fig. 1.

The boundary conditions would lead to an infinite set of equations. To make the problem tractable, boundary conditions will be satisfied only at a finite number of points on the boundary. The infinite series are truncated to form a square-matrix equation on the coefficients of basis functions. Since this equation is homogeneous, the determinant must vanish.

Combined with (5) and (6), the determinant equation gives the phase constant of propagating modes. Let us emphasize that the required number of basis functions is affected by the symmetry and the smoothness of the boundary geometry.

In this paper, we adopt the Goell's scheme [4] and designate propagation modes as E_{mn}^x or E_{mn}^y according to the direction of the electric field vector in the high frequency limit. This method of denoting modes is con-

venient when boundary shape has symmetry and becomes difficult when the boundary lacks symmetry.

The refraction index of the optical fiber is denoted as n_1. The difference between the refraction index of the optical fiber and vacuum is denoted as Δn_1. That is,

$$n_1 = \frac{k_1}{k_0} \tag{13}$$

$$\Delta n_1 = n_1 - 1. \tag{14}$$

The propagation constant β is normalized as

$$p^2 = \frac{(\beta/k_0)^2 - 1}{n_1^2 - 1} \tag{15}$$

and the optical frequency is also normalized as

$$A = \frac{2a}{\lambda_0}\sqrt{n_1^2 - 1} \tag{16}$$

where a is the maximum diameter of a fiber.

III. Results of Computation

A. Types of Treated Boundaries

Fig. 2 shows several types of boundaries treated in our computation. The ellipse (a) can be analyzed most easily by this method because it is smooth and has two axes of symmetry. In other words, we only have to treat the first quadrant. The chipped circle (b) also has two symmetry axes but has four corners. Since fields change rapidly near corners, more boundary points should be taken compared with the case of smooth boundaries. The egg shape (c) has a smooth boundary but has only one symmetry axis. An asymmetrical shape (d) is also analyzed.

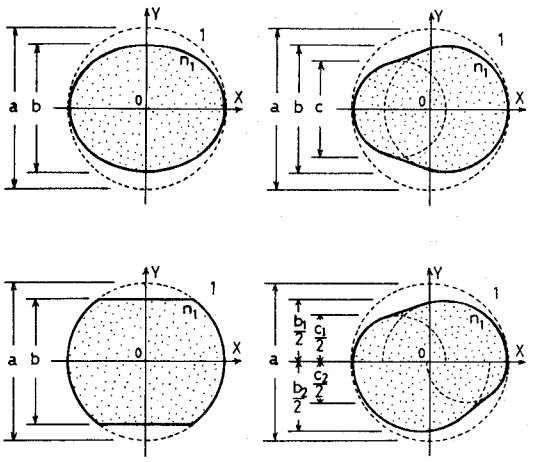

Fig. 2. Types of deformed boundaries. (a) Ellipse. (b) Chipped circle. (c) Egg shape. (d) Asymmetrical shape.

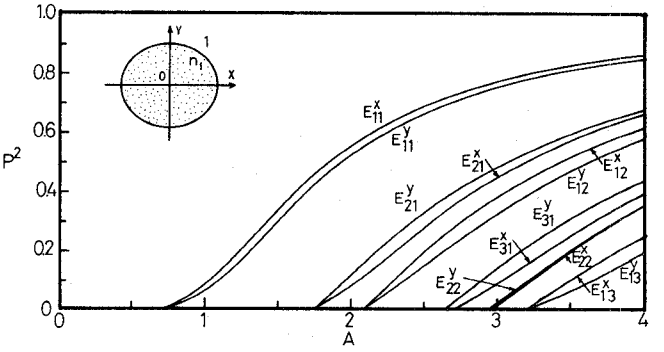

Fig. 3. The normalized propagation constant of an elliptical fiber: $b = 0.8a$, $\Delta n_1 = 0.5$.

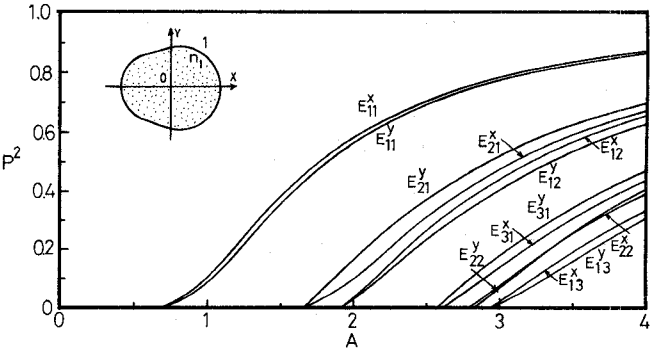

Fig. 4. The normalized propagation constant of an egg-shape fiber: $b = 0.9a$, $c = 0.8b$, $\Delta n_1 = 0.5$.

B. Propagation Constants

Figs. 3 and 4 show the calculated values of P^2 against A for two types of boundaries. It is seen in all of these graphs that the degeneracy of the HE_{11} mode has been lifted by the deformation, and the mode separates into a E_{11}^x mode and a E_{11}^y mode. The TE_{01} and TM_{01} modes of a circular dielectric waveguide are corresponding to the E_{21}^y mode and the E_{21}^x mode, respectively. The degeneracy of the HE_{21} mode is also lifted, and the mode separates into a E_{12}^x mode and a E_{12}^y mode.

C. Number of Basis Functions

The convergence of eigenvalues or the normalized propagation constant P^2 depends on the symmetry and smoothness of the boundaries, as shown in Tables I and II. The dimension of the matrix is four times the number of boundary points. The maximum dimension of matrices permitted by our computer is about 100. This means that the types of boundaries explored in this paper can be easily handled, and P^2 can be obtained with three significant digits. Table III shows typical matrix dimensions.

The computation times for obtaining P^2 from the root of a matrix of dimension M increases exponentially with M. In our computer HITAC-8700, this relation is

$$S = 0.016 \exp(0.062M)(\text{s}). \tag{17}$$

D. Wave Functions

The convergence of an algorithm for wave functions is, in general, slower than for the evaluation of P^2. However, it is important to see if the numerically obtained wave functions are physically reasonable, even if only the propagation constants are required. Fig. 5 illustrates the convergence of the E_z-component in the case of the E_{11}^x mode of the chipped-circle boundary.

E. Field Distribution

When eigenvalues are determined, fields may be obtained. It is an important and interesting fact that the

TABLE I
THE CONVERGENCE OF P^2 BY INCREASING THE NUMBER OF BASIS FUNCTIONS N IN THE CASE OF AN ELLIPTICAL FIBER. $b=0.8a$, $\Delta n_1=0.5$

		P^2			
MODE		E_{11}^y	E_{31}^y	E_{22}^x	E_{13}^y
	A	2.0	4.0	4.0	4.4
N	2	0.5223	0.4424	0.3499	0.3038
	3	0.5225	0.4397	0.3534	0.3010
	4	0.5225	0.4398	0.3538	0.3011
	5	0.5225	0.4399	0.3538	0.3011
	6	0.5225	0.4399	0.3538	0.3011

TABLE II
THE CONVERGENCE OF P^2 BY INCREASING THE NUMBER OF BASIS FUNCTIONS N IN THE CASE OF AN EGG-SHAPE FIBER. $b=0.9a$, $c=0.8b$, $\Delta n_1=0.5$

		P^2			
MODE		E_{11}^y	E_{31}^y	E_{12}^x	E_{21}^y
	A	2.0	4.0	3.2	3.2
N	8	0.5653	0.4668	0.5220	0.6556
	9	0.5722	0.5012	0.5088	0.5573
	10	0.5620	0.5070	0.5022	0.5816
	11	0.5656	0.4783	0.4922	0.5639
	12	0.5678	0.4647	0.4979	0.5624
	13	0.5650	0.4668	0.4966	0.5699
	14	0.5669	0.4677	0.4951	0.5643
	15	0.5651	0.4653	0.4972	0.5651

TABLE III
THE REQUIRED DIMENSION OF MATRICES M FOR VARIOUS BOUNDARIES.

	M	
MODE	DOMINANT	HIGHER ORDER
ELLIPSE	12	16 ~ 20
CHIPPED-CIRCLE	20	28 ~ 32
EGG SHAPE	38	46
ASYMMETRICAL SHAPE	44	48

dominant HE_{11} mode separates into two modes which have different polarizations and no cutoff frequencies. These two polarizations are related to the existence of two independent polarizations of plane waves in free space. Fig. 6 illustrates the pattern of the electric field vectors of these two modes in the cross section.

F. The Phase Constant Difference Between the Two Fundamental Modes

In the fabrication process of optical fibers, the nominally circularly symmetric cross section gets more or less deformed. Therefore, the two fundamental modes E_{11}^x and E_{11}^y have a phase constant difference $\Delta\beta$ [3]. When the two modes are excited at the input of the optical fiber, rotation of the polarization is significant after some length L of fiber. When the deformation of boundaries is small, $\Delta\beta$ is given approximately by

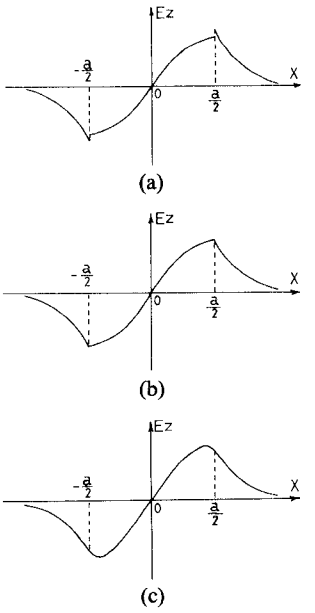

Fig. 5. An illustration of the convergence of wave functions. The distribution of the E_z component on the x axis in the case of the E_{11}^x mode of the chipped-circle fiber: $b=0.8a$, $\Delta n_1=0.5$, $A=2.0$. (a) $N=5$. (b) $N=7$. (c) $N=9$.

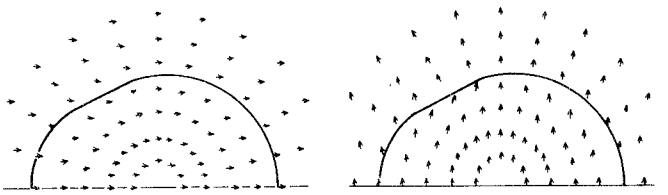

Fig. 6. The direction of electric field vectors in the cross section of an egg-shape fiber: $b=0.9a$, $c=0.8b$, $\Delta n_1=0.5$, $A=2.0$. (a) E_{11}^x mode. (b) E_{11}^y mode.

$$\frac{\Delta\beta}{k_0}=C(A)\Delta n_1^2\cdot\frac{b-a}{2a} \tag{18}$$

in the case of an ellipse or chipped circle where C is a function of A.

Examples of calculated values are

$$C=0.305 \text{ (ellipse, } A=2.0) \tag{19}$$

$$C=0.166 \text{ (chipped circle, } A=2.0). \tag{20}$$

If the parameters of an optical fiber are given by

$$\frac{b-a}{2a}=0.001 \qquad \Delta n_1=0.005 \qquad \lambda_0=1.0\ \mu\text{m} \tag{21}$$

the calculated fiber length L such that

$$\Delta\beta\cdot L=\frac{\pi}{2} \tag{22}$$

is 60 m.

IV. MICROWAVE-MODEL EXPERIMENTS

We tested the accuracy of the numerical data calculated by the above method by microwave-model experiments. Teflon was selected as the dielectric material to form waveguides since its dielectric constant is known and it has no dispersion at microwave frequencies.

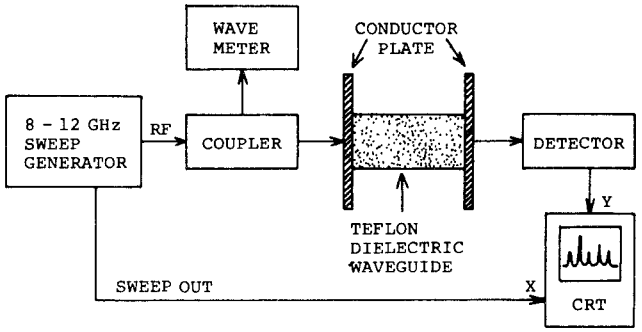

Fig. 7. Experimental setup to measure resonant frequencies of Teflon rod waveguides.

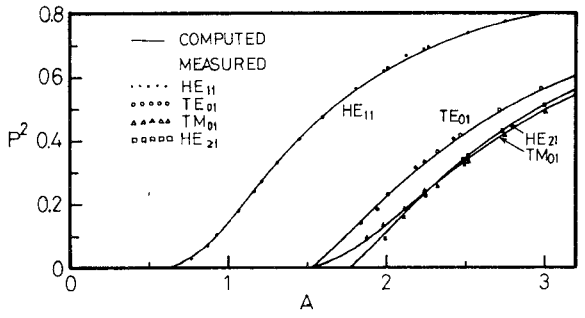

Fig. 8. Comparison of measured values with calculated values of P^2 in the case of a circular dielectric waveguide: $n_1^2=2.04$ (Teflon).

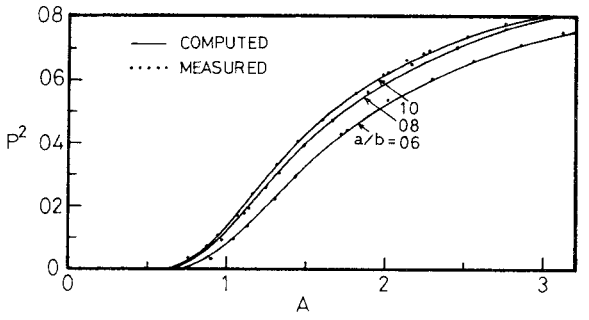

Fig. 9. Comparison of measured values with calculated values of P^2 in the case of the E_{11}^x mode of a chipped-circle dielectric waveguide: $n_1^2=2.04$ (Teflon).

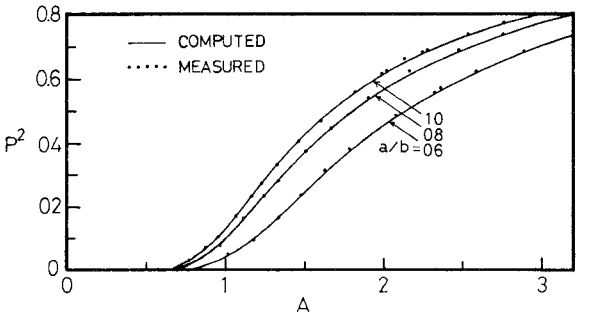

Fig. 10. Comparison of measured values with calculated values of P^2 in the case of the E_{11}^y mode of a chipped-circle dielectric waveguide: $n_1^2=2.04$ (Teflon).

The chipped-circle boundary was selected because it can be fabricated easily. Teflon rods with diameters from 1 to 4 cm were used to make resonators. Resonance frequencies of these resonators were measured at frequencies from 8 to 12 GHz by the experimental setup as shown as the diagram in Fig. 7. The values of P^2 were calculated from these data and plotted in Figs. 8–10.

Fig. 8 shows the case of a circular cross section. Because this has been analyzed rigorously, good agreement between these theoretical and experimental values is a check on the accuracy of the experiments. Figs. 9 and 10 show the gradual change of P^2 for a chipped-circle boundary of increasing deformation.

These experimental results agree well with calculated values. Hence, the numerical analysis described in this paper is considered to be useful for solving deformed-boundary problems.

V. Conclusion

The modal characteristics of homogeneous optical fibers with several types of deformed boundaries were investigated by a numerical method based on point-matching. The propagation constants were obtained with three significant figures. Microwave-model experiments using Teflon waveguides agree well with the calculated values.

A functional-analysis approach would be necessary for investigating precisely the convergence problem in this method. However, the results of computer experiments and microwave-model experiments seem to justify the practical use of this method for analyzing various boundaries close to a circle.

The outside medium was taken to be a vacuum. However, structures consisting of a core fiber and a cladding can be treated easily in similar fashion.

Acknowledgment

The authors thank the cooperation of the Waveguide Line Section, Ibaraki Electrical Communication Laboratory, Nippon Telegraph and Telephone Public Corporation.

References

[1] C. Yeh, "Elliptic dielectric waveguides," *J. Appl. Phys.*, vol. 33, pp. 3235–3243, Nov. 1962.

[2] W. Schlosser, "Die Störung der Eigenwerte des runden dielektrischen Drahtes bei schwacher elliptischer Deformation der Randkontur," *Arch. Elekt. Ubertragung*, band 19, pp. 1–8, Jan. 1965.

[3] ——, "Delay distortion in weakly guiding optical fibers due to elliptic deformation of the boundary," *Bell Syst. Tech. J.*, vol. 51, pp. 487–492, Feb. 1972.

[4] J. E. Goell, "A circular-harmonic computer analysis of rectangular dielectric waveguides," *Bell Syst. Tech. J.*, vol. 48, pp. 2133–2160, Sept. 1969.

[5] J. R. James and I. N. L. Gallett, "Point-matched solutions for propagating modes on arbitrarily-shaped dielectric rods," *Radio Electron. Eng.*, vol. 42, pp. 103–113, Mar. 1972.

[6] T. S. Bird, "A numerical analysis of optical guides with polygonal boundaries," *Proc. IREE—Monitor*, pp. 235–241, July 1976.